DAMAGE DETECTION OF A T-SHAPED PANEL BY WAVE PROPAGATION ANALYSIS IN THE PLANE STRESS

M. RUCKA[1], W. WITKOWSKI[2], J. CHRÓŚCIELEWSKI[3], K. WILDE[4]

A computational approach to analysis of wave propagation in plane stress problems is presented. The initial-boundary value problem is spatially approximated by the multi-node C^0 displacement-based isoparametric quadrilateral finite elements. To integrate the element matrices the multi-node Gauss--Legendre-Lobatto quadrature rule is employed. The temporal discretization is carried out by the Newmark type algorithm reformulated to accommodate the structure of local element matrices. Numerical simulations are conducted for a T-shaped steel panel for different cases of initial excitation. For diagnostic purposes, the uniformly distributed loads subjected to an edge of the T-joint are found to be the most appropriate for design of ultrasonic devices for monitoring the structural element integrity.

Key words: Wave propagation, damage detection, steel T-shaped panel, spectral element method.

1. INTRODUCTION

Wave propagation modelling is a subject of intensive investigations and vast amount of literature is available on this topic. Modelling of wave propagation phenomena might be conducted either in time or frequency domain. One of the frequency-based methods, is the spectral finite element method (SFEM) developed by Doyle [1] and followed by Gopalakrishnan and his co-workers (e.g. [2, 3,]). A different approach is offered by the spectral element method (SEM) developed by Patera [4]. The main idea of the SEM is using a polynomial of high order for each domain. The spectral element method is the same as the *p*-version of the multi-node finite element method [5]. In the SEM approach, the Lagrange-type interpolation polynomials are applied at the Gauss-Legendre-Lobatto nodes. The spectral element method can also be based

[1] Department of Structural Mechanics and Bridge Structures, Faculty of Civil and Environmental Engineering, Gdansk University of Technology, Poland, e-mail: mrucka@pg.gda.pl

[2] Department of Structural Mechanics and Bridge Structures, Faculty of Civil and Environmental Engineering, Gdansk University of Technology, Poland, e-mail: wojwit@pg.gda.pl

[3] Department of Structural Mechanics and Bridge Structures, Faculty of Civil and Environmental Engineering, Gdansk University of Technology, Poland, e-mail: jchrost@pg.gda.pl

[4] Department of Structural Mechanics and Bridge Structures, Faculty of Civil and Environmental Engineering, Gdansk University of Technology, Poland, e-mail: wild@pg.gda.pl

on the Chebyshev polynomials as the basis functions at the Chebyshev-Gauss-Lobatto points [6]. The spectral elements in time domain are available for elementary structural models. The wave propagation in a rod and plane beam elements using the SEM were presented by Kudela *et al.* [7]. The numerical analyses of frame and truss structures can be found in Refs. [8] and [9]. Experimental and numerical analyses of wave propagation in three types of frames, namely an L-frame (a.k.a. L-joint), a T-frame (a.k.a. T-joint) and a portal frame were presented by Rucka in Refs. [10] and [11]. The study of literature reveals that the analysis of wave propagation in plane stress problems (with possible detection of singularities or cracks) is limited to rectangular panels. Żak *et al.* analysed an isotropic panel [12] and a composite panel [13]. Sridhar et al. [6] developed the plane element with Chebyshev nodes for analysis of rectangular beams. Rucka [14] developed the time domain spectral element based on the Kane-Mindlin theory and proved its efficiency on the example of in-plane waves in a rectangular plate measured in 17 points.

In this paper the focus is on computational aspects of the proposed approach. The study is confined to infinitesimal strain case with the linearly elastic homogenous isotropic material. The C^0 finite elements of arbitrary number of nodes are formulated. Element matrices are integrated using the Gauss-Legendre-Lobatto quadrature rule that asserts the diagonal mass matrix. The temporal integration scheme is formulated to take advantage of the structure of element matrices. The developed code is used for wave propagation simulations in the plane stress. The considered geometry consisted of unions of rectangular regions connected along some edges and formed into a T-shaped panel (a.k.a. T-joint) Such example may serve as rough approximation of connection nodes in planar trusses. The paper resumes the authors' studies of damage detection in T-joint by in-plane waves [15]. Results presented in this study are broadened to analysis of six different cases of excited in-plane waves. The purpose of this paper are numerical simulations to determine the suitable excitation for ultrasonic diagnostic device designed for constant monitoring of integrity of the steel T-joint panel.

2. Weak formulation of initial-boundary value problem

The formulation, whether strong or weak, of the initial-boundary value (IBV) problem of the Cauchy continuum may be found in many classical textbooks, cf. for instance [16, 17], and hence it will not be dwelled upon here.

Consider a body B with boundary ∂B of prescribed positive mass density ρ : $B \to \mathbf{R}^1$ experiencing an (infinitesimal) displacement field $\boldsymbol{u}(\boldsymbol{x}, t)$, $\boldsymbol{x} \in B$, $t \in [0, T]$ with given body force vector $\boldsymbol{f} : B \times]0, T[\to \mathbf{R}^{n_{\dim}}$, given boundary traction vector $\boldsymbol{t} : \partial B_f \times]0, T[\to \mathbf{R}^{n_{\dim}}$ and prescribed boundary displacement vector $\bar{\boldsymbol{u}} : \partial B_d \times]0, T[\to \mathbf{R}^{n_{\dim}}$, with $]0, T[$ as the open set. The boundary is understood as usual to be the union $\partial B = \partial B_d \cup \partial B_f$ with $\partial B_d \cap \partial B_f = \emptyset$. The initial conditions are assumed as $\boldsymbol{u}(\boldsymbol{x}, 0) = \boldsymbol{u}_0(\boldsymbol{x})$, $\dot{\boldsymbol{u}}(\boldsymbol{x}, 0) = \boldsymbol{v}_0(\boldsymbol{x})$, $\forall \boldsymbol{x} \in B$, $t = 0$. Here, the superposed dot denotes the

time derivative. The components of vectors and tensors are understood as Cartesian. Under the assumption of infinitesimal deformation considered here, the deformation at given $x \in B$ is described by the infinitesimal strain tensor $\varepsilon = \nabla^s u$.

Let H^1 be the Sobolev space of functions (cf. also [18]), that is $H^1 = H^1(B) = \{w : w \in L_2; \; w_{,x} \in L_2\}$, $L_2(B) = \left\{w : \int_B w^2 dx < \infty\right\}$. Then the space of kinematically admissible displacements is $S = \left\{u : u_i \in H^1; \; u(x) = \bar{u}; \; x \in \partial B_d\right\}$ and the space of kinematically admissible virtual displacements satisfying homogenous boundary conditions is $V = \left\{w : w_i \in H^1; \; w(x) = 0; \; x \in \partial B_d\right\}$. With these definitions the weak form of IBV problem may be stated as follows. Given f, t, $\bar{u}$, u_0 and v_0, find $u(t) \in S_t$, $t \in [0, T]$, such that $\forall w \in V$

$$(2.1) \qquad (w, \rho \ddot{u})_B + (w, c\dot{u})_B + a(\mathbf{w}, \mathbf{u})_B = (\mathbf{w}, \mathbf{f})_B + (\mathbf{w}, \mathbf{t})_{\partial B_f}$$

where c is the positive damping density.

In case of linear elasticity for any given vector fields, say $\mathbf{a}$, $\mathbf{b}$, the above notation reads

$$(2.2) \quad (a, b)_B = \int_B a \cdot b \, \mathrm{d}V, \quad \mathrm{a}\,(a, b)_B = \int_B \nabla^s a \cdot \mathbf{c} \, \nabla^s b \, \mathrm{d}V, \quad (a, b)_{\partial B_f} = \int_{\partial B_f} a \cdot b \, \mathrm{d}s$$

where $\cdot$ is the scalar product. The explicit expressions of bilinear forms from (2.1) will be presented later.

In $(2.2)_2$ $\mathbf{c} \equiv \mathbf{c}(x, n, t)$ denotes the constitutive tensor that, in general, depends on x – the placement and n – the material direction. In the plane stress case $\mathbf{c}$ reads

$$(2.3) \qquad \mathbf{c}_{\alpha\beta\gamma\pi} = \bar{\lambda}\delta_{\alpha\beta}\delta_{\gamma\pi} + \mu\left(\delta_{\alpha\gamma}\delta_{\beta\pi} + \delta_{\alpha\pi}\delta_{\beta\gamma}\right)$$

where Greek letters take values from 1 to 2 while $\mu = \dfrac{E}{2(1 + v)}$ and $\bar{\lambda} = \dfrac{2\lambda\mu}{2\mu + \lambda} = \dfrac{Ev}{1 - v^2}$. Following the argumentation presented in [17], it can be shown that in the isotropic linear elasticity $\mathbf{c}$ in the form of (2.3), in plane stress problems, admits two speeds of propagation of plane elastic waves given by the formulae

$$(2.4) \qquad c_1 = \sqrt{\frac{1}{\rho}\frac{E}{1 - v^2}}, c_2 = \sqrt{\frac{\mu}{\rho}}$$

In the following FEM implementation we write the constitutive equation using the matrix/vector notation

$$(2.5) \qquad \begin{bmatrix} \sigma_{11} \\ \sigma_{22} \\ \sigma_{12} \end{bmatrix} = \frac{E}{1 - v^2} \begin{bmatrix} 1 & v & 0 \\ v & 1 & 0 \\ 0 & 0 & \frac{1}{2}(1 - v) \end{bmatrix} \begin{bmatrix} \varepsilon_{11} \\ \varepsilon_{22} \\ 2\varepsilon_{12} \end{bmatrix}, \quad \boldsymbol{\sigma} = \mathbf{E}\boldsymbol{\varepsilon}$$

3. Finite element method approach

3.1. Spatial approximation and interpolation in plane stress

Following the standard finite element method (FEM) approach, the two-dimensional domain B may be approximated as the sum

$$(3.1) \qquad B \approx \sum_{e \in N_e} B_{(e)}$$

where N_e is the number of finite elements. A typical finite element $B_{(e)}$ is defined as a smooth image of a so-called standard element $\pi_{(e)}$. In the plane stress problem $\pi_{(e)} = [-1, +1] \times [-1, +1]$ is the element in the parent (natural) domain $\boldsymbol{\xi} = (\xi^1, \xi^2)$. It is assumed that the element has $N = m \cdot n$ nodes, where m denotes the number of nodes in ξ^1 direction whereas n in ξ^2 direction, cf. Fig 1.
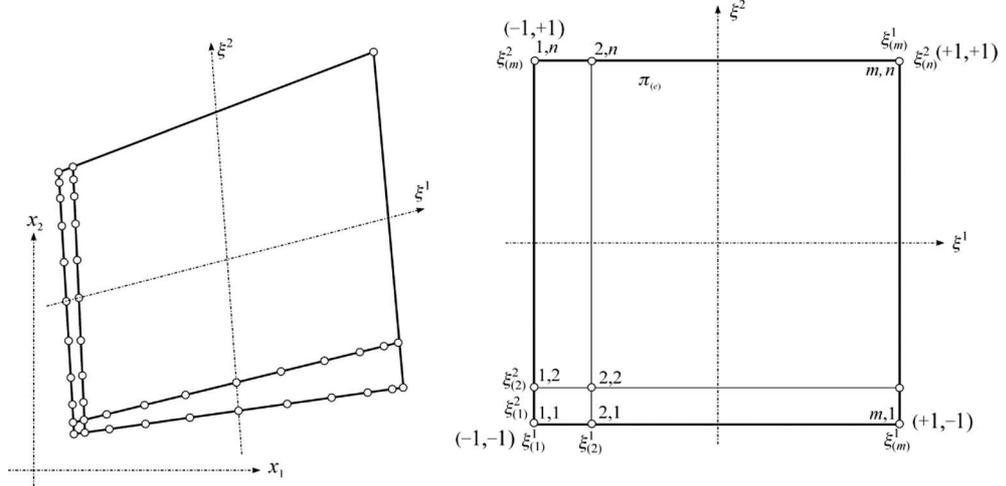

Fig. 1. Standard Lagrange-type interpolation in $\mathbf{R}^2$.
Rys. 1. Interpolacja Lagrange'a w $\mathbf{R}^2$

Let

$$(3.2) \qquad L_p^m(\xi) = \prod_{\substack{q \neq p \\ q=1}}^{m} \frac{\xi - \xi_{(q)}}{\xi_{(p)} - \xi_{(q)}}$$

be the Lagrange polynomial of order $m - 1$. The shape function of the element

$$(3.3) \qquad L_a(\boldsymbol{\xi}) = L_r^{m_1}(\xi^1)\, L_s^{m_2}(\xi^2)$$

results from the rule $g = f(\xi^1, \xi^2)$ associating the number of the element nodes $a, b = 1, 2, ..., N$ with the node numerations $r = 1, 2, ..., m$ and $s = 1, 2, ..., n$ of the interpolation polynomials entering (3.3). The nodal shape functions (3.3) satisfy

$$(3.4) \qquad L_a(\boldsymbol{\xi}_b) = \delta_{ab}, \quad \sum_{a=1}^{N} L_a(\boldsymbol{\xi}) = 1, \quad \forall \boldsymbol{\xi} \in \pi_{(e)}$$

The matrix of C^0 interpolation functions of the a-th node is then

$$(3.5) \qquad \mathbf{L}_a(\boldsymbol{\xi}) = \begin{bmatrix} \mathbf{L}_a(\boldsymbol{\xi}) & 0 \\ 0 & \mathbf{L}_a(\boldsymbol{\xi}) \end{bmatrix}$$

while the matrix of the whole N-node element (e) is $\mathbf{L}_{(e)}(\boldsymbol{\xi}) = [\mathbf{L}_1(\boldsymbol{\xi})|L_2(\boldsymbol{\xi})|...|\mathbf{L}_N(\boldsymbol{\xi})]$. Therefore, the C^0 interpolation scheme for the vector variables of the problem is

$$(3.6) \qquad \mathbf{u}(\boldsymbol{\xi}, t) = \mathbf{L}_{(e)}(\boldsymbol{\xi}) \mathbf{q}_{(e)}(t), \quad \mathbf{q}_{(e)}(t) = \left\{ \begin{array}{c} \mathbf{u}_1(t) \\ \vdots \\ \mathbf{u}_N(t) \end{array} \right\}, \quad \mathbf{u}_a(t) = \left\{ \begin{array}{c} u_1(t) \\ u_2(t) \end{array} \right\}_a$$

For variables independent of time t the time parameter in formulae of the type (3.6) is omitted. In addition, following usual methodology, the strain tensor ε and its virtual counterpart $\delta\varepsilon$ are rewritten as vectors, and in the plane stress problems they are given as

$$(3.7) \qquad \boldsymbol{\varepsilon} \to \boldsymbol{\varepsilon} = \left\{ \begin{array}{c} \varepsilon_{11} \\ \varepsilon_{22} \\ 2\varepsilon_{12} \end{array} \right\} = \boldsymbol{D}\mathbf{u}, \; \delta\boldsymbol{\varepsilon} \to \delta\boldsymbol{\varepsilon} = \left\{ \begin{array}{c} \delta\varepsilon_{11} \\ \delta\varepsilon_{22} \\ 2\delta\varepsilon_{12} \end{array} \right\} = \boldsymbol{D}\mathbf{w}, \; \boldsymbol{D} = \begin{bmatrix} (.),_1 & 0 \\ 0 & (.),_2 \\ (.),_2 & (.),_1 \end{bmatrix}$$

The interpolation schemes are

$$(3.8) \qquad \boldsymbol{\varepsilon}(\boldsymbol{\xi}, t) = \boldsymbol{D}\mathbf{L}_{(e)}(\boldsymbol{\xi}) \mathbf{q}_{(e)}(t) = \mathbf{B}_{(e)}(\boldsymbol{\xi}) \mathbf{q}_{(e)}(t)$$

$$(3.9) \qquad \delta\boldsymbol{\varepsilon}(\boldsymbol{\xi}) = \boldsymbol{D}\mathbf{L}_{(e)}(\boldsymbol{\xi})\delta\mathbf{q}_{(e)} = \mathbf{B}_{(e)}(\boldsymbol{\xi})\delta\mathbf{q}_{(e)}, \; \delta\mathbf{q}_{(e)} = \left\{ \begin{array}{c} w_1 \\ \vdots \\ w_N \end{array} \right\}, \quad w_a = \left\{ \begin{array}{c} w_1 \\ w_2 \end{array} \right\}_a$$

where $\mathbf{B}_{(e)}(\boldsymbol{\xi}) = \boldsymbol{D}\mathbf{L}_{(e)}(\boldsymbol{\xi})$. Assuming that ρ and c are constant over the element, in the light of arbitrariness of $\boldsymbol{w}(\boldsymbol{\xi})$ and with representation (3.6) of the position vector $\boldsymbol{x}(\boldsymbol{\xi})$, the virtual displacement vector $\boldsymbol{w}(\boldsymbol{\xi})$, the displacement vector $\boldsymbol{u}(\boldsymbol{x}, t)$, the velocity vector $\dot{\boldsymbol{u}}(\boldsymbol{x}, t)$, the acceleration vector $\ddot{\boldsymbol{u}}(\boldsymbol{x}, t)$, the body force vector $\boldsymbol{f}(\boldsymbol{x}, t)$ and the prescribed

traction vector $t(x, t)$, $x \in \partial B_f$ the matrix versions of bilinear forms entering (2.1) become

$$(3.10) \qquad a(w, u)_{B_{(e)}} \rightarrow \mathbf{r}_{(e)} = h_0 \int_{B_{(e)}} \mathbf{B}_{(e)}^T(\boldsymbol{\xi})\, \boldsymbol{\sigma}_{(e)}(\boldsymbol{\xi})\, \mathrm{d}x_1 \mathrm{d}x_2$$

$$(3.11) \qquad (w, \rho\ddot{u})_{B_{(e)}} \rightarrow \mathbf{M}_{(e)} = \rho h_0 \int_{B_{(e)}} \mathbf{L}_{(e)}^T(\boldsymbol{\xi})\mathbf{L}_{(e)}(\boldsymbol{\xi})\, \mathrm{d}x_1 \mathrm{d}x_2$$

$$(3.12) \qquad (w, c\dot{u})_{B_{(e)}} \rightarrow \mathbf{C}_{(e)} = c h_0 \int_{B_{(e)}} \mathbf{L}_{(e)}^T(\boldsymbol{\xi})\mathbf{L}_{(e)}(\boldsymbol{\xi})\, \mathrm{d}x_1 \mathrm{d}x_2 = \frac{c}{\rho}\mathbf{M}_{(e)} = \eta\, \mathbf{M}_{(e)}$$

(3.13)

$$(w, f)_{B_{(e)}} + (w, t)\, \partial B_f^{(e)} \rightarrow \mathbf{p}_{(e)}^{\text{elem}} = h_0 \left(\int_{B_{(e)}} \mathbf{L}_{(e)}^T(\boldsymbol{\xi})\, \mathbf{f}(\boldsymbol{\xi})\, \mathrm{d}x_1 \mathrm{d}x_2 + \int_{\partial B_f^{(e)}} \mathbf{L}_{(e)}^T(\boldsymbol{\xi})\, \mathbf{t}(\boldsymbol{\xi})\, \mathrm{d}s \right)$$

where h_0 is the thickness of the body, assumed to be constant throughout the element area. It is assumed that ρ and c are proportional (up to the units) $\eta = c/\rho$, where η denotes a proportional damping coefficient. The element stiffness $\mathbf{K}_{(e)}$ matrix is not used directly in the present formulation. Instead, the internal forces $\mathbf{r}_{(e)}$ are computed according to (3.10). In (3.15) the integrands are defined by

$$(3.14) \qquad \mathbf{f}(\boldsymbol{\xi}, t) = \mathbf{L}_{(e)}(\boldsymbol{\xi})\, \mathbf{f}_{(e)}(t), \; \boldsymbol{\xi} \in \pi_{(e)}, \; \mathbf{f}_{(e)}(t) = \left\{ \begin{array}{c} f_1(t) \\ \vdots \\ f_N(t) \end{array} \right\}, \quad f_a(t) = \left\{ \begin{array}{c} f_1(t) \\ f_2(t) \end{array} \right\}_a$$

and

$$(3.15) \qquad \mathbf{t}(\boldsymbol{\xi}, t) = \mathbf{L}_{(e)}(\boldsymbol{\xi})\, \mathbf{t}_{(e)}(t), \boldsymbol{\xi} \in \partial\pi_{(e)}, \; t_{(e)}(t) = \left\{ \begin{array}{c} t_1(t) \\ \vdots \\ t_N(t) \end{array} \right\}, \quad t_a(t) = \left\{ \begin{array}{c} t_1(t) \\ t_2(t) \end{array} \right\}_a$$

Here $\mathbf{x}_a \in \partial B_f^{(e)}$, $\partial B_f^{(e)} = \partial B_{(e)} \cap \partial B_f \neq \emptyset \quad \partial\pi_{(e)} \leftrightarrow \partial B_{(e)}$. The Jacobian determinant $j(\boldsymbol{\xi}) = \det(\partial \mathbf{x}/\partial \boldsymbol{\xi})$ is

$$(3.16) \qquad j(\boldsymbol{\xi}) = \frac{\partial x_1}{\partial \xi^1}\frac{\partial x_2}{\partial \xi^2} - \frac{\partial x_1}{\partial \xi^2}\frac{\partial x_2}{\partial \xi^1}$$

which renders the transformation formula for the volume area

$$(3.17) \qquad dV = h_0 dA = h_0 dx_1 dx_2 = j(\boldsymbol{\xi}) h_0 d\xi^1 d\xi^2$$

In addition, adhering to the usual FEM approach, it is assumed that the element external load vector $\mathbf{p}_{(e)}^{\text{elem}}$ (3.13) may be supplemented with the vector of point forces applied directly at the element nodes, so that

$$(3.18) \qquad \mathbf{p}_{(e)} = \mathbf{p}_{(e)}^{\text{elem}} + \mathbf{p}_{(e)}^{\text{nod}}, \mathbf{p}_{(e)}^{\text{nod}} = \left\{ \begin{array}{c} \mathbf{P}_1 \\ \vdots \\ \mathbf{P}_N \end{array} \right\}, \mathbf{P}_a = \left\{ \begin{array}{c} P_{x_1} \\ P_{x_2} \end{array} \right\}_a$$

where P_{x_1}, P_{x_2}, analogously to $\mathbf{p}_{(e)}^{\text{elem}}$, are the components referred to the global coordinate system.

In writing the equilibrium condition the following vectors of inertia and damping

$$(3.19) \qquad \mathbf{b}_{(e)} = \mathbf{M}_{(e)}\ddot{\mathbf{u}}_{(e)}, \mathbf{c}_{(e)} = \mathbf{C}_{(e)}\dot{\mathbf{u}}_{(e)}$$

are used. The global equations of motion are obtained in the course of standard aggregation procedure which leads to the matrix form of the equilibrium equation

$$(3.20) \qquad \mathbf{M}\ddot{\mathbf{q}} + \mathbf{C}\dot{\mathbf{q}} = \mathbf{p} - \mathbf{r}(\mathbf{q})$$

Here $\mathbf{q}$, $\ddot{\mathbf{q}}$ and $\dot{\mathbf{q}}$ are the vectors of displacements, accelerations and velocities, respectively. The temporal approximation of dynamic equilibrium equations (3.20) take the advantage of diagonal structure of the matrices.

3.2. NUMERICAL INTEGRATION

The element matrices are evaluated numerically

$$(3.21) \qquad \int_{B_{(e)}} \mathbf{g}(\boldsymbol{x})\,\mathrm{d}x_1\mathrm{d}x_2 = \int_{\pi_{(e)}} \mathbf{g}(\boldsymbol{\xi})j(\boldsymbol{\xi})\,d\xi^1 d\xi^2 = \sum_{p=1}^{M} \mathbf{g}(\boldsymbol{\xi}_p)\, w_p\, j(\boldsymbol{\xi}_p)$$

where $\mathbf{g}(\boldsymbol{\xi})$ represents any quantity from the equations (3.10)-(3.13), M denotes the number of integration points, $p \in 1, 2, \ldots, M$ is the label of $\boldsymbol{\xi}_p = (\xi^1, \xi^2)_p$, i.e. the abscissa, and $w_p = w_{\xi_p^1} \cdot w_{\xi_p^2}$ stands for the associated weight.

Let P^M denote the M-th order Legendre polynomial defined as

$$(3.22) \qquad P^M(\xi) = \frac{1}{2^M M!} \frac{d^M}{d\xi^M}[(\xi^2 - 1)^M], \xi \leftarrow \xi^1,\ \xi^2$$

In the Gauss-Legendre-Lobatto quadrature rule, cf. for instance [5], the abscissas are formally computed as the roots of the equation

$$(3.23) \qquad (1 - \xi^2)\frac{dP^{M-1}(\xi)}{d\xi} = 0, M \leftarrow m, n$$

whereas the weights follow from

$$(3.24) \qquad w = \frac{2}{M(M-1)(P^{M-1}(\xi))^2}, M \leftarrow m, n$$

Although the number of integration points is the same as the number of element nodes, the integration rule used here cannot be termed 'full integration' since it can easily be checked that the mass matrix is underintegrated. Thus the stiffness matrix is integrated exactly while the mass matrix is integrated non-exactly. The inexact integration by the Gauss-Legendre-Lobatto quadrature effectively diagonalizes the mass matrix [19]. Diagonal mass matrix integrated in such a way is said to be optimally lumped [20].

3.3. Temporal approximation

The temporal integration is performed by the method described in details in Refs. [8] and [9]. Following the standard argumentation, cf. for instance [16], solution of the linear equation of motion (3.20) is approximated by $\mathbf{q}_n \equiv \mathbf{q}(t_n)$ in the finite number of time points $t_1, t_2, ..., t_n, ..., t_i < t_{i+1}$. Assuming that $\mathbf{q}_n$, $\dot{\mathbf{q}}_n$ and $\ddot{\mathbf{q}}_n$ are known from the previous step, the solution at the next time point $t_{n+1} = t_n + \Delta t$ is predicted by

$$(3.25) \qquad \mathbf{M}\ddot{\mathbf{q}}_{n+1} + \mathbf{C}\dot{\mathbf{q}}_{n+1} = \mathbf{p}_{n+1} - \mathbf{r}(\mathbf{q}_{n+1})$$

where Δt is the time step. The presence of $\mathbf{q}_{n+1}$ on rhs of (3.25) makes the scheme implicit and iterations are required. Assuming Newmark's approximations [20] in iterative notation (see [8]), the implicit equation wrt iteration correction $\delta\ddot{\mathbf{q}}$ reads

$$(3.26) \qquad [\mathbf{M} + \Delta t \gamma \mathbf{C}]\delta\ddot{\mathbf{q}} = \mathbf{p}_{n+1} - \mathbf{b}_{n+1}^{(i)} - \mathbf{c}_{n+1}^{(i)} - \mathbf{r}\left(\mathbf{q}_{n+1}^{(i)} + (\Delta t)^2\beta\delta\ddot{\mathbf{q}}\right)$$

Equation (3.26) is solved using the simple iteration method leading to

$$(3.27) \qquad \delta\ddot{\mathbf{q}} = [\mathbf{M} + \Delta t \gamma \mathbf{C}]^{-1}\left(\mathbf{p}_{n+1} - \mathbf{b}_{n+1}^{(i)} - \mathbf{c}_{n+1}^{(i)} - \mathbf{r}(\mathbf{q}_{n+1}^{(i)})\right)$$

In view of the fact that $\mathbf{M}$ and $\mathbf{C}$ are diagonal, significant efficiency of the time integration scheme is attained.

4. Simulations of wave propagation in T-shaped panel

4.1. Description of T-shaped panel and FE model

The considered T-joint panel is shown in Fig. 2. The panel consists of two elements. The horizontal part has length of 1 m and height of 0.2 m. The attached vertical element has a length of 0.4 m, counted from the connection with the horizontal element. All the

members are made of steel and have thickness of 0.005 m. The steel of the T-joint has modulus of elasticity E = 196.58 GPa, mass density ρ = 7976 kg/m^3 and Poisson's ratio v = 0.27. Simulations of propagating waves are performed for two cases: the T-shaped panel without any defect and the panel with a defect in the form of a hole of squared shape of 0.04 m by 0.04 m located at the distance of 0.44 m from the left-down corner of the panel. The area of the defect is 0.0016 m^2, which is about 0.6% of the total area of the panel equal 0.28 m^2.
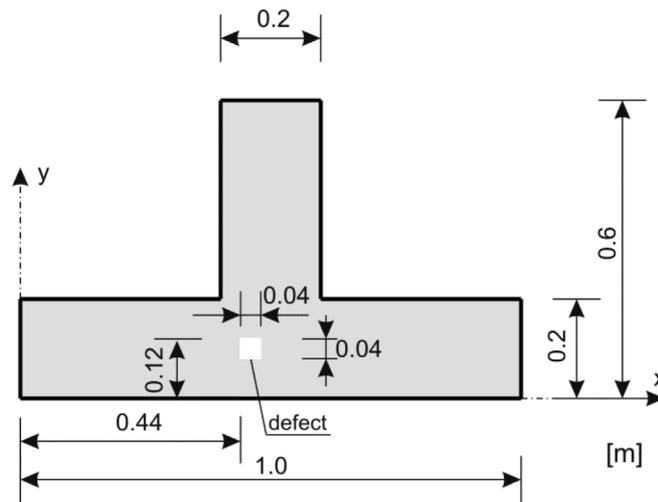
Fig. 2. Geometry of T-shaped joint and location of the defect.
Rys. 2. Geometria tarczy typu T oraz położenie defektu

The spectral FE model of the T-joint is shown in Fig. 3. The panel is divided into 175 square elements of size 0.04 m by 0.04 m. The single element has 11×11 nodes. Such element has been chosen as a compromise between the multi-node approach and the sufficiently large integration time step. An odd number of nodes per element side is preferred since it provides a node in the middle of each element side. The panel has no external supports and the boundary conditions are assumed to be free, i.e. all the nodes located along the edges of the T-joint are not restricted in any direction. The FE model of the T-joint has 17901 nodes and 35802 degrees of freedom. The time step has been chosen as $\Delta t = 10^{-7}$ s. The applied time step has been selected in view of the numerical stability criteria of the central difference method. The computational effort for the single simulation of wave propagation in terms of CPU time was about 25 minutes (the hardware used for simulations was HP notebook, 4 GB RAM, Intel Core2 (Duo) running at 2.5 GHz under Windows XP).

As the excitation a four-cycle sinusoidal wave of frequency 120 kHz modulated by Hanning window (Fig. 4a) has been used. Different types of excitation waves have been examined. The selected excitation signal compromises the effectiveness of the
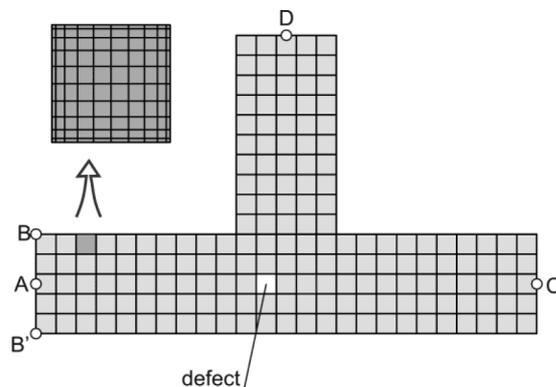
Fig. 3. FEM mesh of T-joint.
Rys. 3. Podział tarczy typu T na elementy skończone

diagnostics and the ability to detect the defects located in the vicinity of the excitation source. In general, using more cycles in the excited wave and wider window result in narrower spectrum. On the other hand, the width of the window in the time domain should be relatively small to enable the observation of wave reflections from potential defects located near the excitation point.
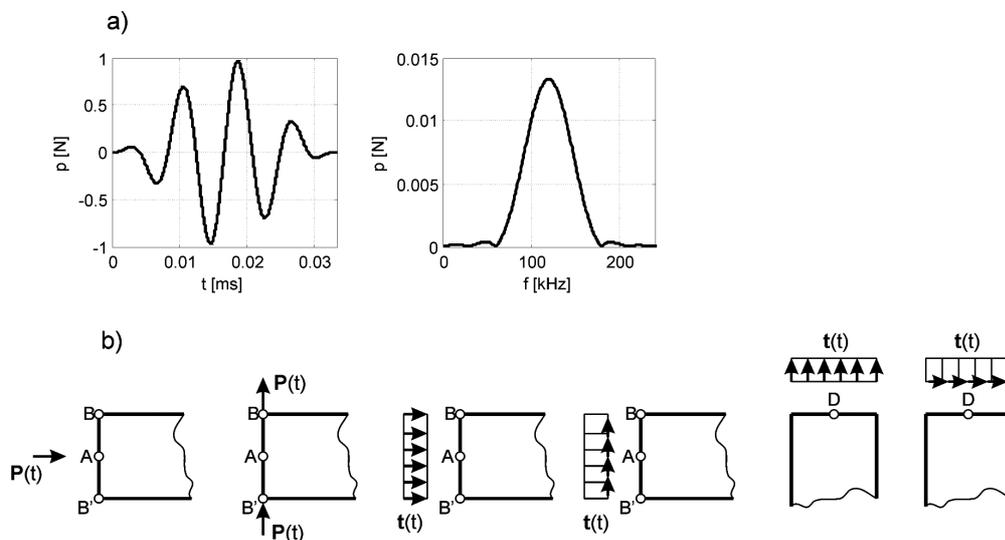

Fig. 4. External excitation: a) excitation function and its Fourier transform, b) types and location of loads.
Rys. 4. Obciążenie zewnętrzne: a) funkcja wzbudzenia oraz jej transformata Fouriera, b) typy i miejsca przyłożenia obciążenia

The propagating waves are simulated for different types, locations and directions of the external excitation. Two types of loads are considered, namely the nodal excitation load $\boldsymbol{P}(t)$ and the uniformly distributed excitation $\boldsymbol{t}(t)$ along the selected edge of the panel (Fig. 4b). In addition, the point or given edge can be excited in the direction perpendicular or parallel to the element edge.

4.2. Wave propagation induced by single point excitation

The single nodal load $\boldsymbol{P}(t)$ was applied in the longitudinal direction at the node A. The wave propagation in terms of acceleration component along the axis x, for both the undamaged panel and the panel with the defect, is illustrated in Fig. 5. Application
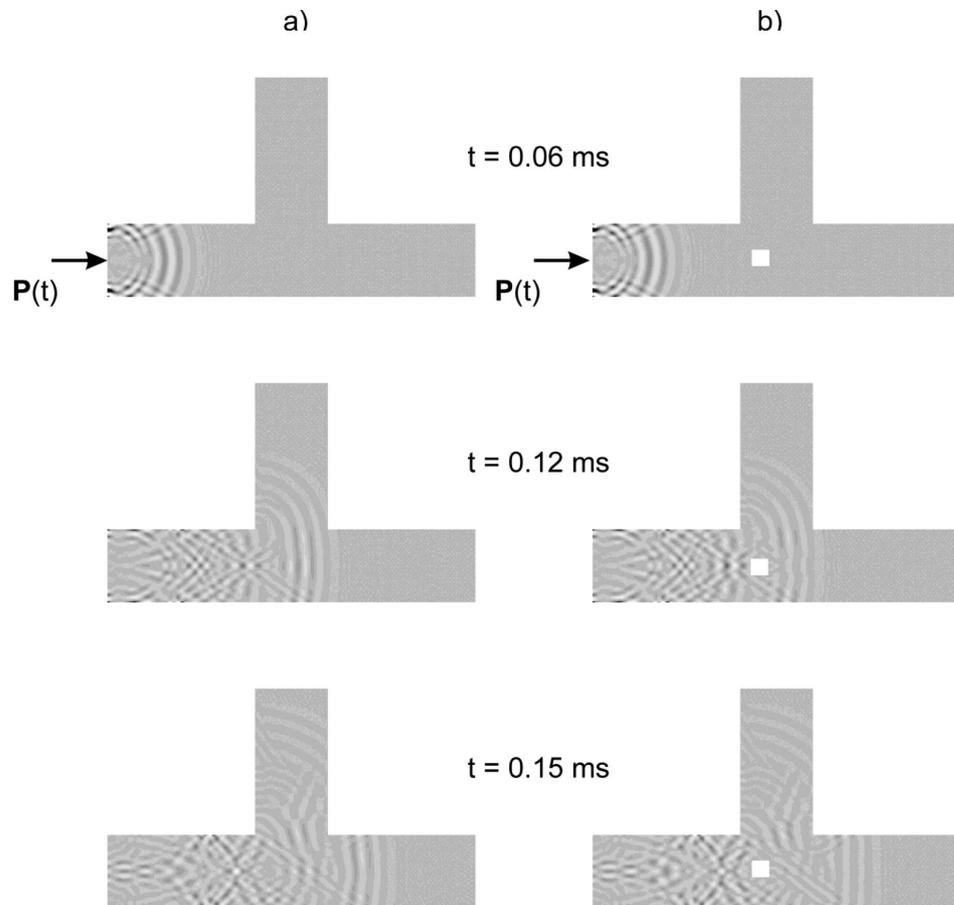
Fig. 5. Propagation of longitudinal wave in the T-shaped panel in the case of single longitudinal excitation force (a) undamaged panel, (b) panel with defect.
Rys. 5. Propagacja fali podłużnej w tarczy typu T w przypadku wzbudzenia punktowego w kierunku podłużnym: (a) tarcza bez uszkodzenia, (b) tarcza z defektem

of the load at the single point results in propagation of the wavefront in the shape of a circle. The shape of the incident wave can be observed at time $t = 0.06$ ms (Fig. 5a). However, the wave patterns behind the initial wavefront, located between the wavefront and the edge $B - B'$, are very complicated due to multiple reflections from all the horizontal panel edges. The wavefront at $t = 0.15$ ms, for the undamaged case, preserves its circular shape. Waves are also propagating in the vertical element of the joint in the upward direction.

The wave propagation through the T-joint with the defect is given in Fig. 5b. The initial wavefront at time $t = 0.06$ ms is identical with the undamaged case. At time $t = 0.12$ ms the wavefront passes the defect. Although some reflections from the defect have occurred, the vertical acceleration distribution within the panel is very similar to the undamaged case. At time $t = 0.15$ ms the incident wavefront is travelling in the right hand side element of the joint. Minor differences in the shape of the wavefront are visible.

The time histories of the accelerations at the point A, in direction along the axis x, are given in Fig. 6. Subtraction of the acceleration of the damaged panel from the record for the undamaged case indicate differences. However, the exposed differences have very small amplitudes.
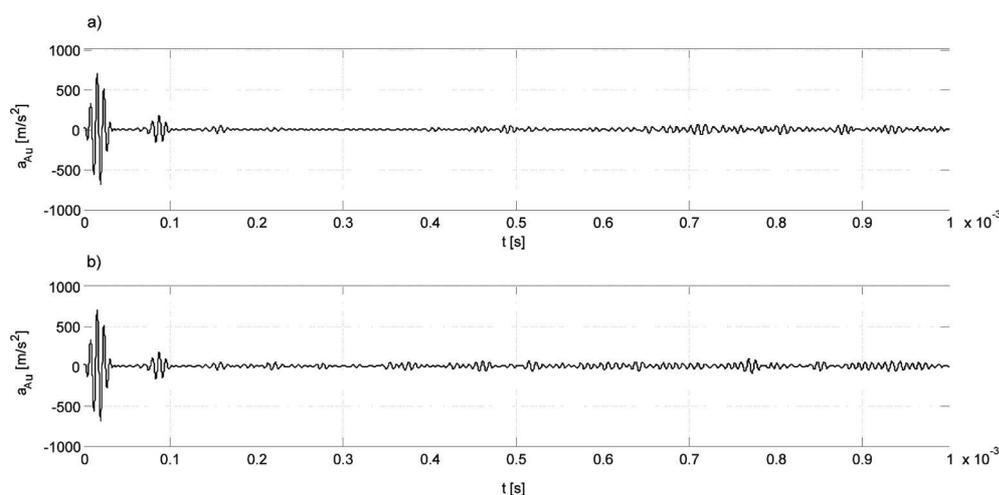

Fig. 6. Acceleration time signals in the node A of the T-shaped panel in the case of single longitudinal excitation force: (a) undamaged panel (b) panel with defect.
Rys. 6. Sygnał przyspieszenia w węźle A w przypadku wzbudzenia punktowego w kierunku podłużnym: (a) tarcza bez uszkodzenia, (b) tarcza z defektem

The second case concerns the nodal load $\boldsymbol{P}(t)$ applied in the direction along the axis y, at the nodes B and B'. The acceleration component along y direction in the undamaged and damaged panel are given in Fig. 7. The acceleration time histories computed at the point B are plotted in Fig. 8. As in the previous case, the acceleration

time history does not explicitly indicate either the defect presence or the defect location. Complicated reflection patterns mask the direct reflections from the defect that could be used for its detection.
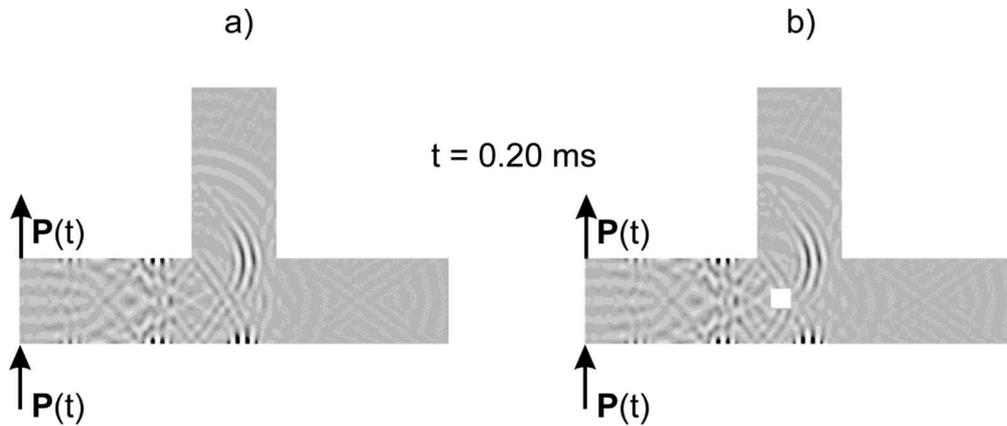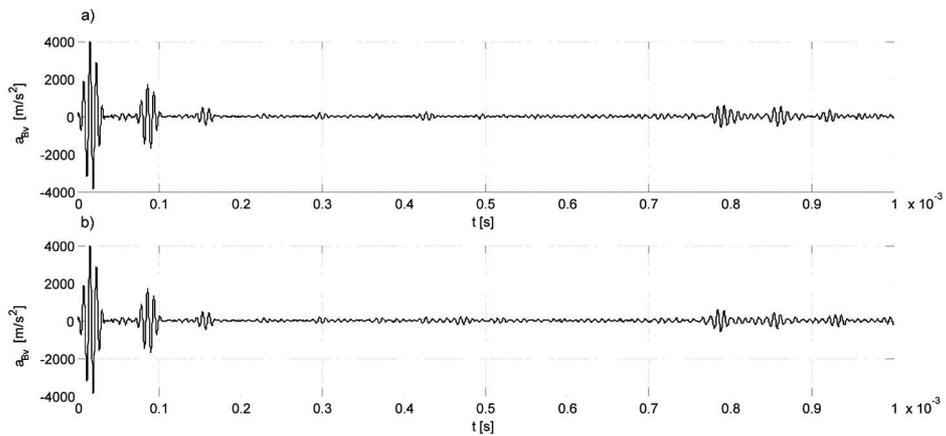

Fig. 7. Propagation of transverse wave in the T-shaped panel in the case of single transverse excitation force: (a) undamaged panel, (b) panel with defect.
Rys. 7. Propagacja fali poprzecznej w tarczy typu T w przypadku wzbudzenia w postaci pojedynczych sił w kierunku poprzecznym: (a) tarcza bez uszkodzenia, (b) tarcza z defektem

Fig. 8. Acceleration time signals in the node A of the T-shaped panel in the case of single transverse excitation force: (a) undamaged panel, (b) panel with defect.
Rys. 8. Sygnał przyspieszenia w węźle A w przypadku wzbudzania w postaci pojedynczych sił w kierunku poprzecznym: (a) tarcza bez uszkodzenia, (b) tarcza z defektem

4.3. Wave propagation induced by uniformly distributed loads

The uniformly distributed loads $t(t)$ are imposed along the x direction on the whole left T-joint edge (the node A belongs to this edge). The acceleration component along the x axis, for the undamaged and damaged panel is given in Fig. 9. The wavefront at $t = 0.06$ ms for the undamaged T-joint (Fig. 9a) can be approximated by a line. Moreover, its amplitude in the whole considered time period is significantly larger than that of the waves resulting from the horizontal edge reflections. The wavefront remains its shape after passing the connection with the vertical panel element (at $t = 0.12$ ms).
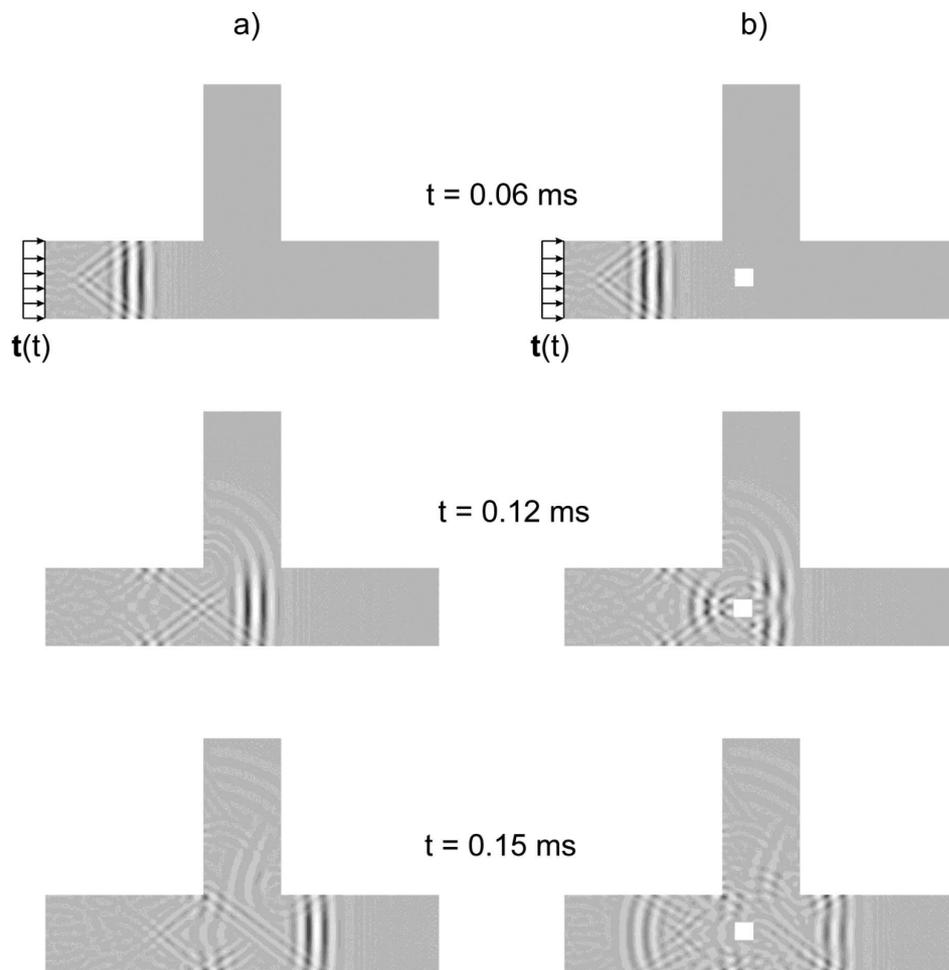
Fig. 9. Propagation of longitudinal wave in the T-shaped panel in the case of linearly distributed longitudinal loads: (a) undamaged panel, (b) panel with defect.

Rys. 9. Propagacja fali podłużnej w tarczy typu T w przypadku podłużnego wzbudzenia równomiernie rozłożonego wzdłuż krawędzi: (a) tarcza bez uszkodzenia, (b) tarcza z defektem

Fig. 9b shows the accelerations for the case of the damaged T-joint. At time $t = 0.12$ the reflection from the defect is clearly visible and its wavefront travels towards the point A. At $t = 0.15$ ms the reflected wave front has a circular shape that is similar to the wave front generated when the point load is applied.
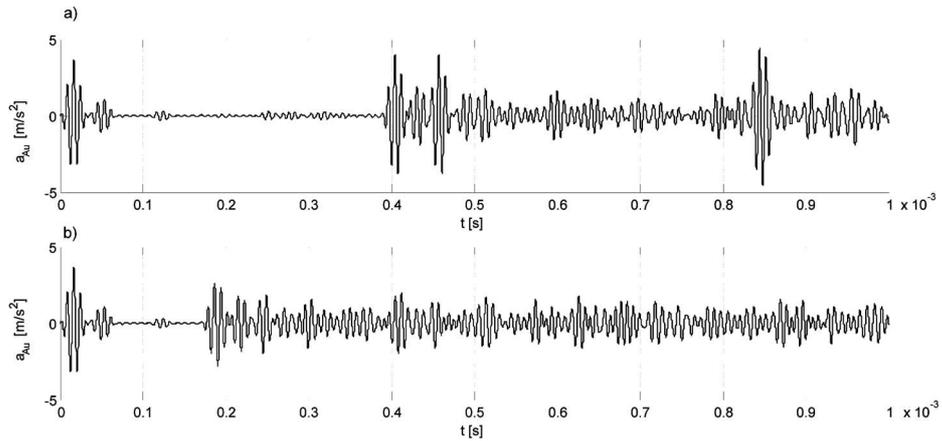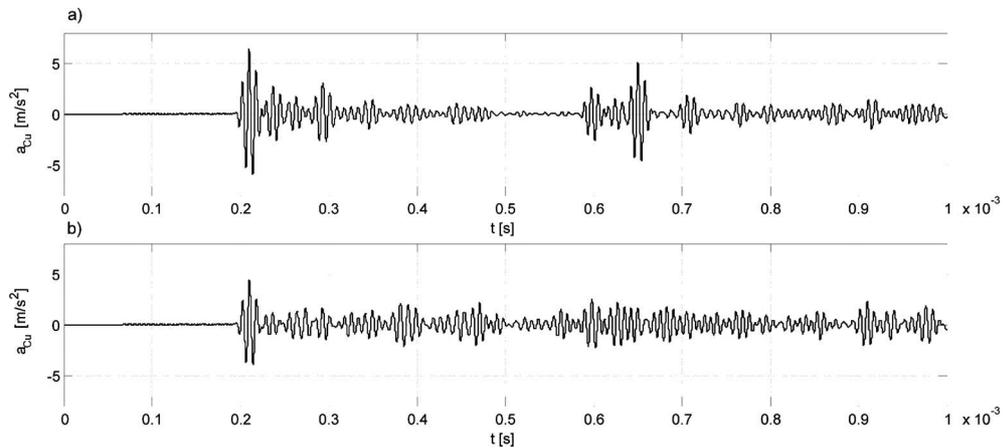

Fig. 10. Acceleration time signals at the node A of the T-shaped panel in the case of linearly distributed longitudinal loads: (a) undamaged panel, (b) panel with defect.
Rys. 10. Sygnał przyspieszenia w węźle A w przypadku podłużnego wzbudzenia równomiernie rozłożonego wzdłuż krawędzi: (a) tarcza bez uszkodzenia, (b) tarcza z defektem

Fig. 11. Acceleration time signals at the node C of the T-shaped panel in the case of linear distributed longitudinal loads: (a) undamaged panel; (b) panel with defect.
Rys. 11. Sygnał przyspieszenia w węźle C w przypadku podłużnego wzbudzenia równomiernie rozłożonego wzdłuż krawędzi: (a) tarcza bez uszkodzenia, (b) tarcza z defektem

The accelerations time histories of the undamaged and damaged panels at the nodes *A* and *C* are given in Fig. 10 and Fig. 11, respectively. In the case of the uniformly distributed excitation, the presence and location of the defect can be easily calculated. The acceleration of the damaged joint at the point *A* shows arrival of the wave of large amplitude, reflected from the defect at the time of about 0.2 ms. The time required to travel from the point *A* to the defect and back allows, for known wave velocity, simple calculation of the defect location. However, the presence of the defect cannot be computed from accelerations at the point *C*. The time histories for the undamaged and damaged panel are different, but the only clear indication of the defect is the change of amplitudes of the wavefront arriving at the point *C*.

In the next example, the uniformly distributed excitation is imposed in the *y* direction along the edge with the node *A*. The transverse wave for the undamaged panel has also the distinct wavefront, which, in its middle part, can be represented by a line (Fig. 12a). The wave propagation in the damaged T-joint is given in Fig. 12b. The reflection from the defect is clearly visible.
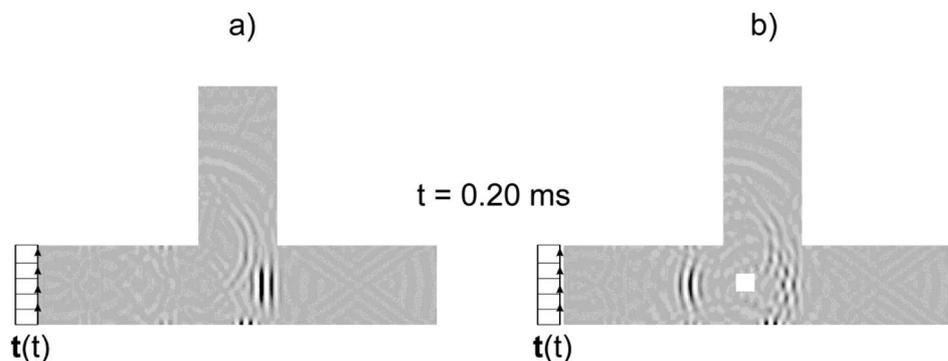

Fig. 12. Propagation of transverse wave in the T-shaped panel in the case of linearly distributed transverse loads: (a) undamaged panel, (b) panel with defect.
Rys. 12. Propagacja fali podłużnej w tarczy typu T w przypadku poprzecznego wzbudzenia równomiernie rozłożonego wzdłuż krawędzi: (a) tarcza bez uszkodzenia, (b) tarcza z defektem

The time histories of the vertical acceleration component are given in Fig. 13 and Fig. 14 for the nodes *A* and *C*, respectively. In this case, the defect location can be computed from accelerations at the points *A* or *C*. The acceleration at the point *A* shows the distinct wave appearing at time 0.3 ms. This wave comes from the reflection from the defect. Knowing the wave velocity for the transverse waves makes the computation of the defect location possible. The defect is also noticeable from the acceleration record at the point *C*. The wave at time about 0.6 ms represents the wave that travels from the point *A* to the point *C*, then reflects itself from the edge, travels to the defect, reflects from the defect, and finally arrives back at the point *C*. The time for this whole trip allows to calculate the defect location. Note that the amplitude of the first wave at the point C is smaller here than the amplitude in the undamaged case.
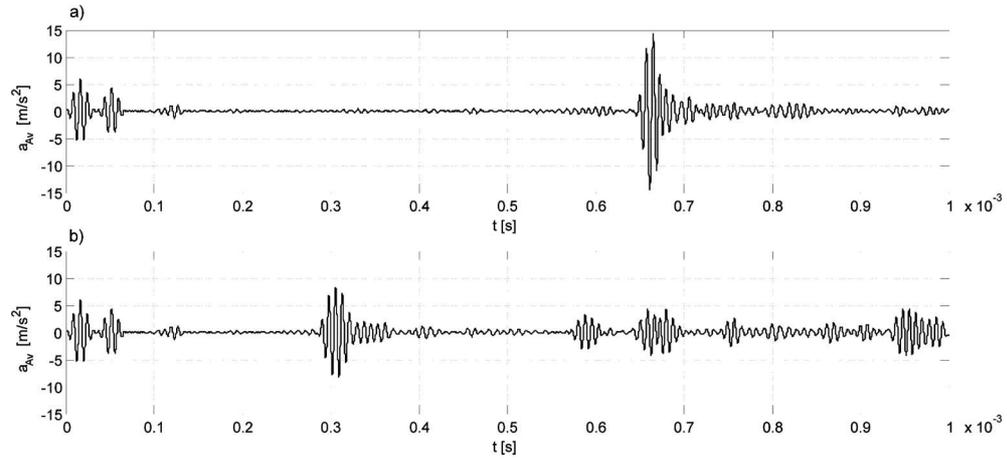
Fig. 13. Acceleration time signals at the node*A* of the T-shaped panel in the case of linearly distributed transverse loads: (a) undamaged panel, (b) panel with defect.
Rys. 13. Sygnał przyspieszenia w węźle *A* w przypadku poprzecznego wzbudzenia równomiernie rozłożonego wzdłuż krawędzi: (a) tarcza bez uszkodzenia, (b) tarcza z defektem
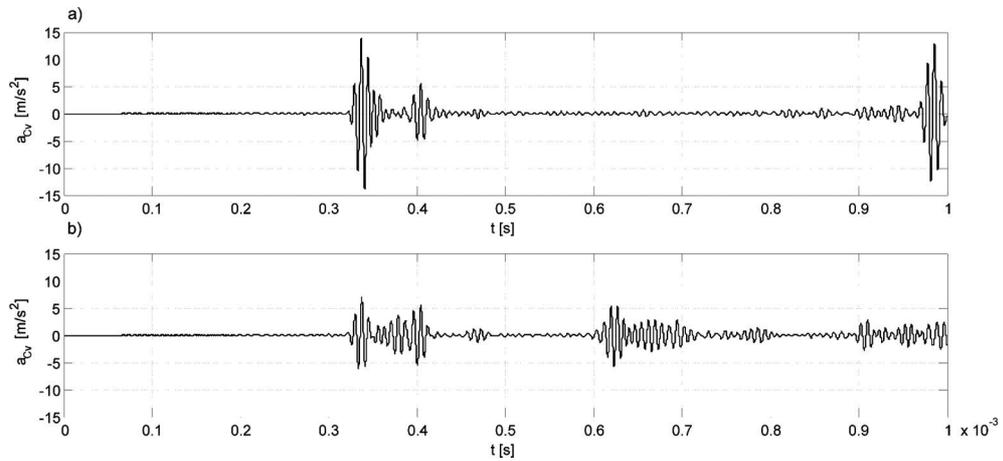

Fig. 14. Acceleration time signals at the node*C* of the T-shaped panel in the case of linear distributed transverse loads: (a) undamaged panel; (b) panel with defect.
Rys. 14. Sygnał przyspieszenia w węźle *C* w przypadku poprzecznego wzbudzenia równomiernie rozłożonego wzdłuż krawędzi: (a) tarcza bez uszkodzenia, (b) tarcza z defektem

The last two examples show the wave propagation for the uniformly distributed excitation placed on the upper edge of the vertical element. Simulation results for excitation in the longitudinal direction (along the *y* axis) is given in Fig. 15 and Fig. 16. As in the previous examples, the wave is travelling mainly within the excited element of the panel. The acceleration response at the point *D*, for the damaged panel shows the arriving wave at time 0.2 ms that appears due to the reflection from the defect.
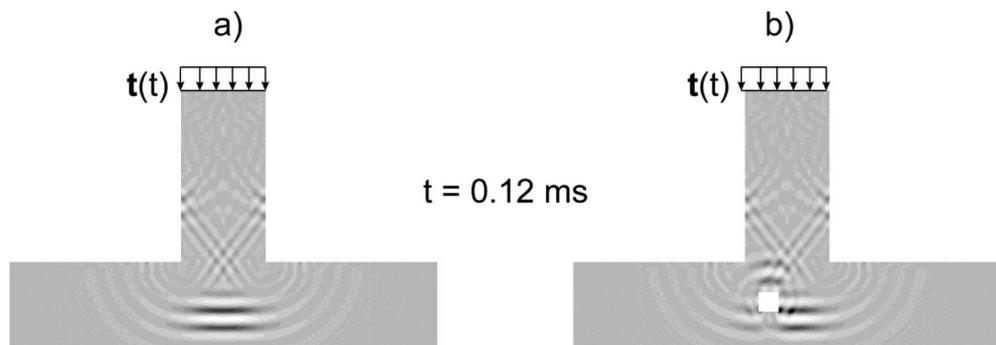

Fig. 15. Propagation of longitudinal wave in the T-shaped panel in the case of linearly distributed longitudinal loads: (a) undamaged panel, (b) panel with defect.
Rys. 15. Propagacja fali podłużnej w tarczy typu T w przypadku podłużnego wzbudzenia równomiernie rozłożonego wzdłuż krawędzi: (a) tarcza bez uszkodzenia, (b) tarcza z defektem
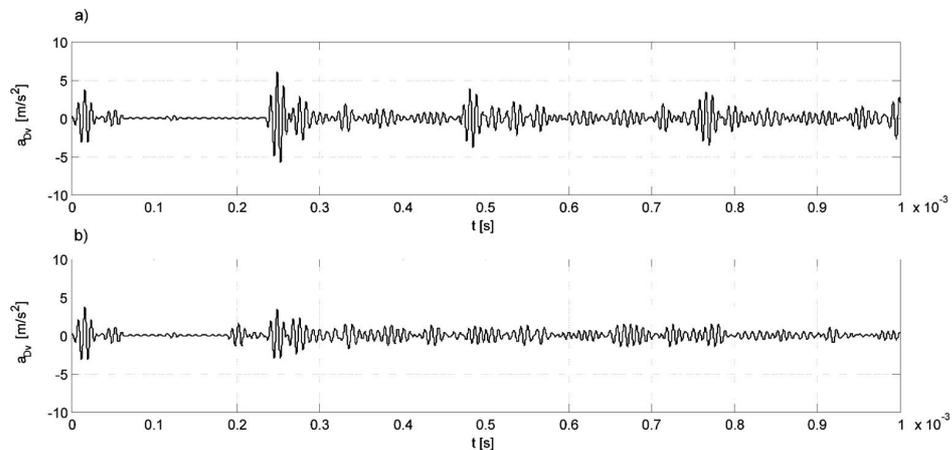

Fig. 16. Acceleration time signals for the T-shaped panel in the case of linearly distributed longitudinal loads: (a) undamaged panel, (b) panel with defect.
Rys. 16. Sygnały przyspieszenia w przypadku podłużnego wzbudzenia równomiernie rozłożonego wzdłuż krawędzi: (a) tarcza bez uszkodzenia, (b) tarcza z defektem

The simulation results for the excitation in the transverse direction, with respect to the vertical element, are given in Fig. 17 and Fig. 18. The acceleration time history at the point D indicates the defect position since the reflected wave at time 0.33 ms is recognized.
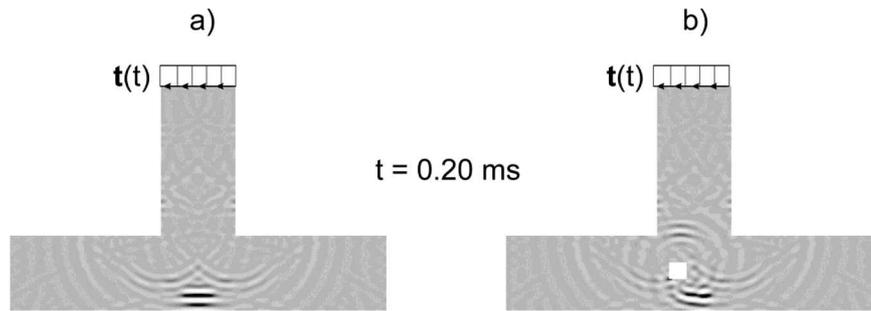

Fig. 17. Propagation of transverse wave in the T-shaped panel in the case of linearly distributed transverse loads: (a) undamaged panel, (b) panel with defect.
Rys. 17. Propagacja fali poprzecznej w tarczy typu T w przypadku poprzecznego wzbudzenia równomiernie rozłożonego wzdłuż krawędzi: (a) tarcza bez uszkodzenia, (b) tarcza z defektem
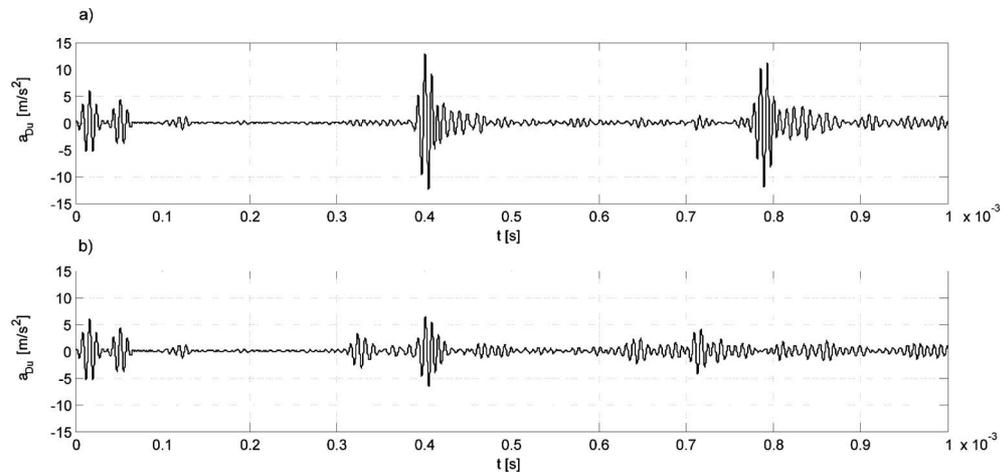

Fig. 18. Acceleration time signals for the T-shaped panel in the case of linearly distributed transverse loads: (a) undamaged panel, (b) panel with defect.
Rys. 18. Sygnały przyspieszenia w przypadku poprzecznego wzbudzenia równomiernie rozłożonego wzdłuż krawędzi: (a) tarcza bez uszkodzenia, (b) tarcza z defektem

5. Conclusions

In this paper, simulations of the wave propagation with assumption of the plane stress for damage detection in the T-joint panel were studied. The presented formulation and the numerical results support the following conclusions:

– the temporal integration conducted by the dedicated integration scheme is sufficiently efficient for the analyzed T joint panel;

– the spectral elements with Gauss-Legendre-Lobatto nodes for the plane stress model allows to simulate and trace complicated phenomena of the elastic wave propagation in the T-joint panels;

– the element matrices are integrated with the quadrature rule in which the number of integration points equals the number of element nodes; therefore, the mass matrix is always diagonal with all the elements positive.

– application of the load in the form of modulated waves imposed at the structure single point cannot be used for effective damage detection method;

– the simulations have shown that the application of the excitation uniformly distributed along the selected edge of the joint provide the effective damage detection method;

– for a reliably defect detection it is necessary to generate a wavefront with a linear shape. In such a case the reflections from the defect significantly affect the wave patterns making the defect detection possible;

– the effective diagnostic method requires a distinct wave fronts, with relatively large amplitudes with respect to the secondary reflected waves,

– a proper selection of the sensor location improves the search of the defect location. For T-joint, the most effective is application of the transverse excitation uniformly distributed at the joint edge (both receivers at A and C give information on the defect location).

Future numerical analyses for the damage detection systems based on guided waves in steel joints should be directed to a more realistic modelling of the joint damage as well as to search of the optimal transducers placement.

Acknowledgements

References

1. J.F. Doyle, *Wave propagation in structures: spectral analysis using fast discrete Fourier transforms* (second ed.). Springer-Verlag, New York 1997.

2. S. Gopalakrishnan, A. Chakraborty, D.R. Mahapatra, *Spectral finite element method: wave propagation, diagnostics and control in anisotropic and inhomogeneous structures*. Springer-Verlag, London 2008.

3. D.S. Kumar, D.R. Mahapatra, S. Gopalakrishnan, *A spectral finite element for wave propagation and structural diagnostic analysis of composite beam with transverse crack*, Finite Elements in Analysis and Design **40**, 1729-1751, 2004.

4. T. Patera, *A spectral element method for fluid dynamics: laminar flow in a channel expansion*. Journal of Computational Physics **54**, 468-488, 1984.

5. C. Canuto, M.Y. Hussaini, A. Quarteroni, T.A. Zang, *Spectral Methods in Fluid Dynamics*, Springer Verlag, Berlin, Heidelberg 1998.

6. R. Sridhar, A. Chakraborty, S. Gopalakrishnan, *Wave propagation analysis in anisotropic and inhomogeneous uncracked and cracked structures using pseudospectral finite element method*. International Journal of Solids and Structures **43**, 4997-5031, 2006.

7. P. Kudela, M. Krawczuk, W. Ostachowicz, *Wave propagation modelling in 1D structures using spectral finite elements*. Journal of Sound and Vibration, **300**, 88-100, 2007.

8. J. Chróścielewski, M. Rucka, K. Wilde, W. Witkowski, *Formulation of spectral truss element for guided waves damage detection in spatial steel trusses*. Archives of Civil Engineering **55**(1), 43-63, 2009.

9. W. Witkowski, M. Rucka, K. Wilde, J. Chróścielewski, *Wave propagation analysis in spatial frames using spectral Timoshenko beam elements in the context of damage detection*. Archives of Civil Engineering **55**, 367-402, 2009.

10. M. Rucka, *Experimental and numerical study on damage detection in an L-joint using guided wave propagation*. Journal of Sound and Vibration **329**, 1760-1779, 2010.

11. M. Rucka, *Wave Propagation in Structures*. Modelling, Experimental Studies and Application to Damage Detection, Gdansk University of Technology Publishers, Series: Monographs no. 106, Gdansk 2011.

12. A. Żak, M. Krawczuk, W. Ostachowicz, *Propagation of in-plane wave in an isotropic panel with a crack*. Finite Elements in Analysis and Design **42**, 929-941, 2006.

13. A. Żak, M. Krawczuk, W. Ostachowicz, *Propagation of in-plane wave in a composite panel with a crack*. Finite Elements in Analysis and Design **43**, 145-154, 2006.

14. M. Rucka, *Modelling of in-plane wave propagation in a plate using spectral element method and Kane-Mindlin theory with application to damage detection*. Archive of Applied Mechanics **81**, 1877-1888, 2011.

15. J. Chróścielewski, M. Rucka, K. Wilde, W. Witkowski, *Modelowanie propagacji fal sprężystych w tarczy typu T w kontekście możliwości diagnostycznych* (in Polish), Biuletyn Wojskowej Akademii Technicznej **60**(1), 341-349, 2011.

16. T.J.R. Hughes, *The Finite Element Method: linear static and dynamics finite element analysis*. Dover Publications, Inc., New York 2000.

17. J.E. Marsden, T.J.R. Hughes, *Mathematical foundations of elasticity*. Dover Publications, Inc., New York 1994.

18. D. Braess, *Finite elements*. Theory, fast solvers and applications in solid mechanics. Cambridge University Press 2007.

19. C. Pozrikidis, *Introduction to Finite and Spectral Element Methods using MATLAB*®. Chapman & Hall/CRC 2005.

20. R.D. Cook, D.S. Malkus, M.E. Plesha, *Concepts and Applications of Finite Element Analysis*, 3rd ed. New York: John Wiley & Sons 1989.

21. N.N. Newmark, *A method of computation for structural dynamics*. Proc ASCE, J. Engng. Mech. Div. 85 (EM3), 1959.

22. O.C. Zienkiewicz, R.L. Taylor, *The Finite Element Metod*, Butterowort-Heienmann, 2000.

WYKRYWANIE USZKODZEŃ W TARCZY TYPU T Z UŻYCIEM ANALIZY
PROPAGACJI FAL W PŁASKIM STANIE NAPRĘŻENIA

S t r e s z c z e n i e

W pracy zaprezentowano podejście obliczeniowe do analizy propagacji fal w płaskim stanie naprężenia. Problem brzegowo-początkowy podlega przestrzennej aproksymacji z użyciem wielowęzłowych, izoparametrycznych, czworobocznych elementów klasy C^0. Macierze elementowe są całkowane numerycznie za pomocą kwadratury Gauss-Legendre-Lobatto. Aproksymację w dziedzinie czasu wykonano za pomocą algorytmu Newmarka. Symulacje numeryczne przeprowadzono dla tarczy w kształcie litery T dla różnych przypadków wzbudzania fali. W pracy wykazano, że dla celów diagnostyki najlepszym rodzajem obciążenia jest obciążenie liniowe równomiernie przyłożone do krawędzi tarczy.